Structurally Uniform Nanosheets Hot Paper

DOI: 10.1002/ange.201403780

Structurally Homogeneous Nanosheets from Self-Assembly of a Collagen-Mimetic Peptide**

*Tao Jiang, Chunfu Xu, Xiaobing Zuo, and Vincent P. Conticello**

Abstract: *A collagen-mimetic peptide, NSIII, has been designed with three sequential blocks having positive, neutral, and negative charges, respectively. The non-canonical imino acid, (2S,4S)-4-aminoproline (amp), was used to specify the positive charges at the Xaa positions of (Xaa-Yaa-Gly) triads in the N-terminal domain of NSIII. Peptide NSIII underwent self-assembly from aqueous solution to form a highly homogeneous population of nanosheets. Two-dimensional crystalline sheets formed in which the length of the peptide defined the height of the sheets. These results contrasted with prior results on a similar multi-domain collagen-mimetic polypeptides in which the sheets had highly polydisperse distribution of sizes in the (x/y)- and (z)-dimensions. The structural differences between the two nanosheet assemblies were interpreted in terms of the relative stereoelectronic effects of the different aminoproline derivatives on the local triple helical conformation of the peptides.*

Recently, we described the design of a collagen-mimetic peptide, NSI, that self-assembled into structurally defined nanosheets.[1] The sequence of peptide NSI encompassed three sequential blocks of identical length with complementary electrostatic properties comprising positively charged, neutral, and negatively charged (Xaa-Yaa-Gly) triads (Figure 1 a).[1–3] The positively charged, non-canonical imino acid, (2*S*,4*R*)-4-aminoproline (Amp),[4,5] was placed at the Yaa positions of the first block to direct Coulombic interactions between oppositely charged residues located on structurally adjacent triple helices. The underlying structure of the NSI nanosheets was based on perpendicular packing of antiparallel oriented collagen triple helices into a two-dimensional tetragonal lattice (see below).[1] However, the resultant nanosheets were highly polymorphic in both the lateral, that is, sheet-growth, dimension and the vertical, that is, sheet-stacking dimension. The wide dispersion in nanosheet sizes is a challenge to the development of applications for these materials as two-dimensional (2D) nanoarchitectonic structural platforms.[6] We describe herein a modification of the NSI sequence to create a peptide, NSIII, which self-assembles into nanosheets that display homogeneity in both lateral sheet dimension and thickness (Figure 1 a).

a) **NSI:** (Pro-Amp-Gly)$_4$–(Pro-Hyp-Gly)$_4$–(Glu-Hyp-Gly)$_4$
NSIII: (amp-Hyp-Gly)$_4$–(Pro-Hyp-Gly)$_4$–(Pro-Glu-Gly)$_4$

b)

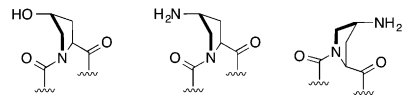

(4*R*)-Hyp (4*R*)-Amp (Amp) (4*S*)-Amp (amp)

Figure 1. a) Amino acid sequences of peptides NSI and NSIII. b) Structures and preferred ring pucker conformers of imino acid derivatives.

The sequence of peptide NSIII differs from the corresponding sequence of NSI in that the epimeric non-canonical imino acid (2*S*,4*S*)-4-aminoproline (amp) was employed in place of (2*S*,4*R*)-4-aminoproline (Amp) as the positively charged residue (Figure 1 b). These two imino acids display preferences for opposite ring puckers, Cγ-*endo* and Cγ-*exo*, respectively, of the pyrrolidine side-chain.[4,5] Crystallographic analyses of collagen model peptides have indicated that the most common conformation for imino acid residues at the Xaa and Yaa positions are the Cγ-*endo* ring pucker and the Cγ-*exo* ring pucker, respectively.[7–9] Therefore, the amp residue in the sequence of NSIII was encoded within the Xaa positions of the respective triad sequences. To compensate, the glutamic acid (Glu) residues were moved to Yaa positions of NSIII. The tri-block architecture of peptide NSI sequence was strictly maintained in NSIII such that direct structural comparisons could be made between these two peptide systems.

Peptide NSIII was synthesized using microwave-assisted solid-phase peptide synthesis and purified by preparative HPLC (see the Supporting Information). Circular dichroism spectropolarimetry (CD) was employed to assess the conformation and thermodynamic stability of peptide NSIII in solution under conditions identical to those that promoted self-assembly of peptide NSI (Figure 2). Peptide NSIII (4 mg mL^{-1}) in MOPS buffer (20 mM, pH 7.0) displayed the classic spectroscopic signature of the collagen triple helix with a minimum at 198 nm and a maximum at 224 nm. Surprisingly, the melting temperature (T_M) of NSIII was only slightly lower (28 °C) than that of NSI (32 °C) under identical conditions, which differs from the previously observed influence of similar substitutions on the thermal stability of collagen-

[*] T. Jiang, Dr. C. Xu, Prof. V. P. Conticello
Department of Chemistry, Emory University
1515 Dickey Drive, Atlanta, GA 30322 (USA)
E-mail: vcontic@emory.edu
Homepage: http://conticellolab.wordpress.com/
Dr. X. Zuo
X-ray Science Division, Argonne National Laboratory
9700 South Cass Avenue, Argonne, IL 60439 (USA)

[**] V.P.C. acknowledges financial support from NSF grant CHE-1012620. This work benefited from the use of the A.P.S. funded by U.S. D.O.E. Office of Basic Energy Sciences, Division of Material Sciences, under contract W-31-109-Eng-38. We thank Prof. Shuming Nie for use of the dynamic light scattering instrument.

Supporting information for this article is available on the WWW under http://dx.doi.org/10.1002/anie.201403780.

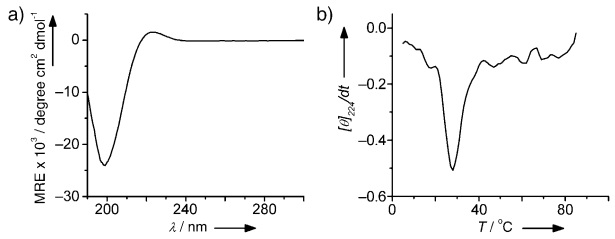

Figure 2. a) Circular dichroism spectra of peptides NSIII (4 mg mL^{-1}) in MOPS buffer (20 mM, pH 7.0). b) First derivative of the CD signal at 224 nm as a function of temperature. The T_M of 28 °C was estimated from the minimum in the first derivative of the melting curve.

mimetic model peptides.[4,10–13] The triple helical secondary structure of NSIII developed over a period of several days in aqueous solution, as judged by the increase in intensity of the CD signal at 224 nm. However, the position of the cooperative melting transition remained constant (Supporting Information, Figure S3), which suggested that triple helix formation coincided with a higher order self-assembly process, as observed previously for peptide NSI.[1]

TEM image analysis (Figure 3a and b) demonstrated that peptide NSIII (4 mg mL^{-1}) self-assembles into nanosheets at 4 °C from MOPS buffer (20 mM, pH 7.0); conditions that are similar to those employed for self-assembly of nanosheets from peptide NSI.[1] However, in contrast to the assemblies observed previously for NSI, a homogeneous population nanosheets was observed for NSIII. Measurement of the diagonal length across the nanosheet surface indicated a narrow range of values for the NSIII assemblies (mean distance = 679 ± 57 nm), which was interpreted as an indication of the homogeneity of the assemblies (Supporting Information, Figures S4, S5). In comparison, a very broad distribution of sheet diagonal values (1–15 μm) was measured for the corresponding NSI nanosheets.

AFM analysis was employed to estimate the height of nanosheets of NSIII. A thickness of 9.6 ± 0.4 nm was observed for the NSIII nanosheets (Figure 3c, d), which compared well to the value of 8.8 ± 0.8 nm measured for single-layer nanosheets of NSI. A theoretical sheet thickness of 10.3 nm (36 residues × 0.286 nm rise/residue for collagen triple helices)[14] was calculated for single-layer nanosheets of NSI and NSIII, which correlates well with the height values measured from tapping-mode AFM imaging under dry conditions. The AFM data support a structure for the NSIII nanosheets in which collagen triple helices pack into a single layer without stacking in the z-direction. In contrast, a wide dispersion of height values (10–250 nm) is observed from AFM measurements on the NSI nanosheets.[1] These results suggested that multi-layer nanosheets are the norm for NSI, while all of the observed NSIII nanosheets corresponded to single layers of collagen triple helices.

TEM and AFM image analysis indicated that the nanosheets formed over a concentration range from 2–10 mg mL^{-1} in MOPS buffer. Moreover, the lateral size of the nanosheets did not vary significantly within this concentration range. The population of nanosheets appeared to increase with time in a manner commensurate with the increase in the intensity of the CD signal. Lower initial concentrations of NSIII ($\leq$ 0.5 mg mL^{-1}) did not support nanosheet formation. Dilution of nanosheets (4 mg mL^{-1}) to non-permissive concentrations (0.25 mg mL^{-1}) resulted in their dis-assembly with concomitant diminution of the CD signal (Supporting Information, Figure S6).

Dynamic light scattering (DLS) measurements of the NSIII nanosheets confirmed this observation, in that a narrow distribution of nanosheets was observed in solution under the self-assembly conditions (Figure 4a). While the Stokes–Einstein relationship does not obtain for two-dimensional objects, the population of nanosheets could still be fit to a single curve that was consistent with a uniform size distribution of self-assembled species. The temperature profile of the dynamic light scattering response indicated that both the intensity of scattered light and the apparent hydrodynamic radius (R) underwent a sharp transition as the temperature increased through the T_M of the collagen triple helix. The observed transition was consistent with dis-

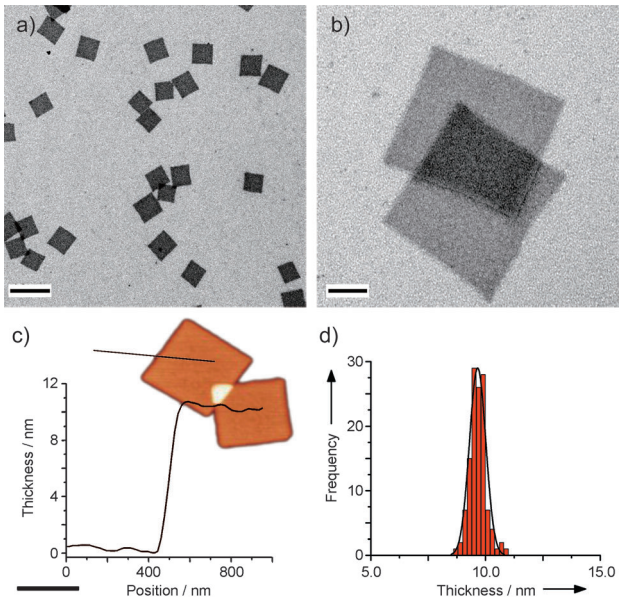

Figure 3. a) TEM image of NSIII nanosheets at low magnification (scale bar = 1 μm). b) TEM image of NSIII nanosheets at high magnification (scale bar = 150 nm). c) Representative AFM image and height profile of a single-layer nanosheets of NSIII (scale bar = 300 nm). d) AFM height histogram for single-layer sheets of NSIII.

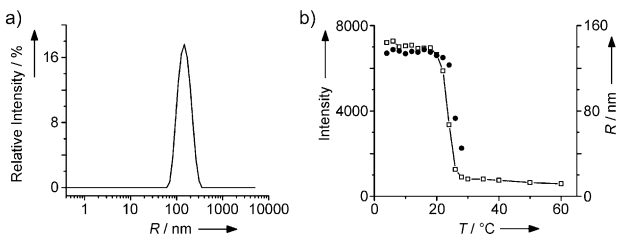

Figure 4. a) Dynamic light scattering measurement of a solution of NSIII nanosheets (2 mg mL^{-1}) in MOPS buffer (20 mM, pH 7.0) at 4 °C. b) Temperature dependence of the scattered light intensity (□) and calculated hydrodynamic radius (●) for a solution of NSIII nanosheets (2 mg mL^{-1}) in MOPS buffer (20 mM, pH 7.0).

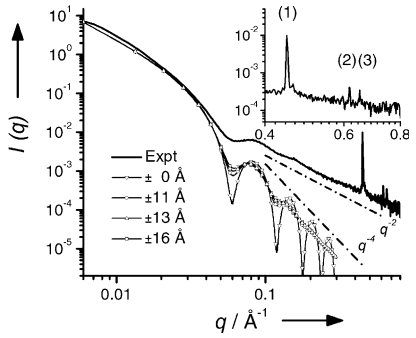

Figure 5. Synchrotron SAXS scattering profile (solid line) for a solution of NSIII sheets (4 mg mL^{-1}) in MOPS buffer (20 mM, pH 7.0) and simulated SAXS profiles using a disc model with homogenous density. To simplify the simulations, the radius of disc was set to 3000 Å, comparable to the sheet surface dimensions measured by TEM. The disc height was set to follow a normal Gaussian distribution centered at 107 Å with different standard deviations (σ). The curve with a value for σ equal to 13 Å has similar level of attenuation on the oscillations as the experimental data. In the Porod region, the disc model with uniform electron density results in a q^{-4} dependence[15] in the simulated curves, while the experimental data show roughly q^{-2} dependence[16] (probably due to a significant contribution from internal structure (non-uniform electron density), which further damps the oscillations). Inset: expansion of the three diffraction peaks in the high q region. Peaks (d-spacing): (1), 14.0 Å; (2), 10.2 Å; and (3), 9.67 Å.

assembly of the nanosheets into individual non-associated NSIII peptides owing to melting of the triple helices.

Synchrotron SAXS/WAXS analysis (Figure 5) of a dilute solution of NSIII displayed a scattering intensity profile that was similar to that observed for nanosheets of NSI. Form-factor scattering was convoluted with sharp peaks that could be attributed to Bragg diffraction in the high q, that is, small d-spacing, region of the scattering curve. The data in the Guinier region ($q_{max}R_c \leq 1.0$) could be fit to a model for sheet-like forms.[15] A value of 107 ± 4 Å for the sheet thickness can be calculated from the Guinier plot (Supporting Information, Figure S7), which compares well to the height from AFM measurements as well as the length of the NSIII peptide projected onto a collagen triple helix (see above). In contrast, the polydispersity of the NSI nanosheets precluded determination of the sheet thickness from Guinier analysis of the SAXS data. The oscillating features in the q range of 0.02–0.3 Å^{-1} arise from the thickness dimension of the nanosheet and provide information on sheet thickness and its distribution. The position of the first oscillation minima is ca. 0.058–0.060 Å^{-1}, corresponding to a thickness of 105–108 Å.[15] The attenuation of the scattering oscillation indicates a dispersion on the thickness, which is estimated no more than ± 13 Å, the standard deviation of a normal Gaussian distribution (Figure 5).

The Bragg diffraction peaks observed in the high q region of the intensity plot support a high degree of internal order for the nanosheets, albeit with a different internal structure than observed for NSI sheets. For the NSI nanosheets, diffraction peaks were observed in the scattering curve at q values of 0.405 Å^{-1} and 0.573 Å^{-1}, which correspond to azimuthally averaged d-spacings of 15.5 Å and 11.0 Å.[1] These d-spacings were interpreted in terms of a tetragonal 2D lattice, which was confirmed with electron diffraction. In comparison, three diffractions peaks were observed in the SAXS scattering profile of the NSIII nanosheets at q values of 0.448 Å^{-1} (d = 14.0 Å), 0.617 Å^{-1} (d = 10.2 Å), and 0.650 Å^{-1} (d = 9.67 Å). The inequivalent values of the latter two spacings and the geometrical relationship between the three d-spacings suggested that NSIII does not pack into the same tetragonal lattice as NSI. Electron diffraction confirmed the lattice spacing (14 Å) of the major diffraction lattice (Figure 6a), although the diffraction patterns from isolated sheets could not be observed due to sheet overlap and sensitivity to radiation damage. A structural model for the NSIII nanosheets was constructed from this data (Figure 6b). This model compares well to that for the NSI nanosheets with the exception that the 2D-lattice of the NSIII nanosheets is slightly distorted from tetragonal and the unit lattice undergoes contraction with respect to the NSI nanosheets (d_{110}: 14 Å for NSIII and 15.5 Å for NSI nanosheets, respectively).[1]

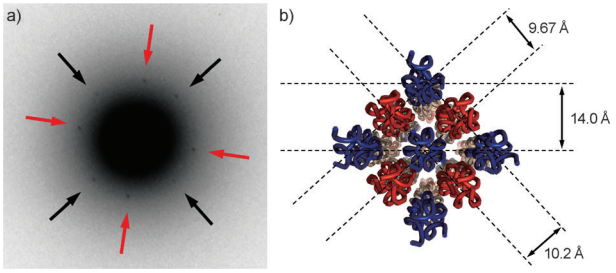

Figure 6. a) Electron diffraction pattern for two overlapping NSIII nanosheets. Diffraction spots were observed at 14.0 Å for each of the two major lattices (red and black arrows). b) Structural model of the 2D lattice for the NSIII nanosheets indicating the d-spacings of planes associated with the packing of triple helices. The collagen triple helices pack in an anti-parallel orientation in which the *N*-terminal positively charged triads (blue) of one triple helix interact selectively with the *C*-terminal negatively charged triads (red) of an adjacent triple helix.

The structural homogeneity of the NSIII nanosheets is striking in comparison to the polydispersity of the corresponding NSI nanosheets. The difference in nanosheet morphology between NSI and NSIII must be attributable to the relatively minor differences in amino acid sequence between the respective peptides. The imino acids (2*S*,4*S*)-4-aminoproline (amp) and (2*S*,4*R*)-4-aminoproline (Amp) posit different ring puckers, Cγ-endo and Cγ-exo, respectively, within small-molecule model compounds.[4,5] These ring puckers are compatible with the preferred conformations of the pyrrolidine rings of the imino acid residues at the Xaa ($\chi_1 \approx 25°$) and Yaa ($\chi_1 \approx -25°$) positions, respectively, within the collagen triple helical structure.[9] Although high-resolution structural information is not available for collagen-mimetic peptides containing either Amp or amp residues, the structure of a collagen-mimetic peptide [(Pro-Hyp-Gly)$_4$(hyp-Pro-Gly)$_2$(Pro-Hyp-Gly)$_4$], **1**, has been determined crystallographically in which the isosteric (2*S*,4*S*)-4-hydroxyproline (hyp) and (2*S*,4*R*)-4-hydroxyproline (Hyp) residues occupy Xaa and Yaa positions, respectively, within a triple helix.[17]

The Hyp residues in peptide **1** display a nearly ideal Cγ-exo ring pucker ($\chi_1 \approx -25°$), as observed previously in a number of reported structures of collagen-mimetic peptides.[7–9] In contrast, the hyp residues display considerable conformational heterogeneity. A significant percentage of hyp residues (ca. 30%) within the structural model for **1** adopt the stereoelectronically unfavorable Cγ-exo ring pucker at the Xaa position. The remaining hyp residues adopt a structurally distorted Cγ-endo ring pucker ($\chi_1 \approx 16°$), presumably to alleviate a sterically unfavorable interaction between the γ-hydroxy group and the pyrrolidine ring of a Hyp residue on a structurally adjacent peptide within the triple helix.

In analogy to the Hyp residues at the Yaa positions in the sequence of peptide **1**, the stereoelectronically similar Amp residues within NSI should adopt a Cγ-exo ring pucker that favors a typical triple helical collagen conformation. Conversely, the amp residues in the Xaa positions of NSIII should recapitulate the conformational properties of the hyp residues of peptide **1**, which would result in stereoelectronically or sterically unfavorable confinement of the substituted pyrrolidine rings with concomitant structural distortion of the triple helix. The conformational differences between the respective triple helices should manifest themselves in terms of differences in electrostatic interactions between charged residues on adjacent protomers within the 2D lattices of NSIII relative to NSI.

We propose that the difference in morphology between the NSI and NSIII nanosheets can be understood in terms of the geometric requirements for packing of the chiral rod-like protomers within the respective 2D lattices. Self-assembly in each case coincides with the formation of the triple helical structure (see above). The extent of self-association depends on a balance between the Coulombic energy of attraction between oppositely charged residues and the energy penalty associated with distortion of the local triple helical conformation to promote packing into the 2D lattice.

In the case of the NSIII nanosheets, local conformational distortion of the triple helix occurs due to the presence of the amp residues. The dimensions of the 2D lattice of the NSIII nanosheets suggest that closer contact between triple helical protomers may be required to promote the optimal electrostatic interactions. Of note in this regard, the 2D lattice of NSIII is contracted in comparison not only to the NSI nanosheets but also to pseudotetragonal crystal structures of collagen model peptides.[9,18] The resultant crystalline order cannot be sustained over large dimensions and frustrates lateral growth as well as sheet stacking. Energetic arguments based on geometrical packing requirements have been invoked to account for restrictions in the dimensions of para-crystalline peptide-based assemblies, including the homogeneity of lateral diameter in type I collagen fibers[19] and synthetic α-helical coiled-coil assemblies[20] as well as the finite degree of lamination of β-sheet fibrils.[21] In contrast, the local triple helical conformation of NSI should be subject to less significant structural distortion owing to the presence of the stereoelectronically preferred Amp residue. As a consequence, the triple helical protomers of NSI undergo minimal distortion owing to the geometrical packing requirements of the 2D lattice, which should promote lateral growth and subsequent sheet stacking.

In summary, the disparity in morphology between NSI and NSIII nanosheets suggests that the geometrical requirements associated with packing of chiral protomers can exert a significant influence on the structure of the resultant assemblies.[22] Manipulation of these quaternary interactions may represent an effective mechanism to control the structure and function of synthetic self-assembled materials. Sequence-defined and structurally regular peptide-based materials manifest complex, owing to the complexity of interactions that are manifested, offer a rich test-bed to explore the implications of this hypothesis.

Received: March 27, 2014
Published online: June 24, 2014

Keywords: collagen-mimetic peptides · nanoarchitectonics · nanosheets · self-assembly · structural homogeneity

[1] T. Jiang, C. Xu, Y. Liu, Z. Liu, J. S. Wall, X. Zuo, T. Lian, K. Salaita, C. Ni, D. Pochan, V. P. Conticello, *J. Am. Chem. Soc.* **2014**, *136*, 4300 – 4308.
[2] S. Rele, Y. Song, R. P. Apkarian, Z. Qu, V. P. Conticello, E. L. Chaikof, *J. Am. Chem. Soc.* **2007**, *129*, 14780 – 14787.
[3] L. E. O'Leary, J. A. Fallas, E. L. Bakota, M. K. Kang, J. D. Hartgerink, *Nat. Chem.* **2011**, *3*, 821 – 828.
[4] a) M. Umashankara, I. R. Babu, K. N. Ganesh, *Chem. Commun.* **2003**, 2606 – 2607; b) I. R. Babu, K. N. Ganesh, *J. Am. Chem. Soc.* **2001**, *123*, 2079 – 2080.
[5] R. S. Erdmann, H. Wennemers, *Angew. Chem.* **2011**, *123*, 6967 – 6970; *Angew. Chem. Int. Ed.* **2011**, *50*, 6835 – 6838.
[6] a) T. Govindaraju, M. B. Avinash, *Nanoscale* **2012**, *4*, 6102 – 6117; b) K. Ariga, Q. Ji, J. P. Hill, Y. Bando, M. Aono, *NPG Asia Mater.* **2012**, *4*, e17.
[7] J. Bella, M. Eaton, B. Brodsky, H. M. Berman, *Science* **1994**, *266*, 75 – 81.
[8] a) R. Berisio, L. Vitagliano, L. Mazzarella, A. Zagari, *Protein Sci.* **2002**, *11*, 262 – 270; b) L. Vitagliano, R. Berisio, A. Mastrangelo, L. Mazzarella, A. Zagari, *Protein Sci.* **2001**, *10*, 2627 – 2632.
[9] a) K. Okuyama, C. Hongo, R. Fukushima, G. Wu, H. Narita, K. Noguchi, Y. Tanaka, N. Nishino, *Biopolymers* **2004**, *76*, 367 – 377; b) N. Jiravanichanun, C. Hongo, G. Wu, K. Noguchi, K. Okuyama, N. Nishino, T. Silva, *ChemBioChem* **2005**, *6*, 1184 – 1187; c) C. Hongo, K. Noguchi, K. Okuyama, Y. Tanaka, N. Nishino, *J. Biochem.* **2005**, *138*, 135 – 144.
[10] a) S. K. Holmgren, K. M. Taylor, L. E. Bretscher, R. T. Raines, *Nature* **1998**, *392*, 666 – 667; b) S. K. Holmgren, L. E. Bretscher, K. M. Taylor, R. T. Raines, *Chem. Biol.* **1999**, *6*, 63 – 70; c) L. E. Bretscher, C. L. Jenkins, K. M. Taylor, M. L. DeRider, R. T. Raines, *J. Am. Chem. Soc.* **2001**, *123*, 777 – 778; d) J. A. Hodges, R. T. Raines, *J. Am. Chem. Soc.* **2003**, *125*, 9262 – 9263.
[11] M. D. Shoulders, F. W. Kotch, A. Choudhary, I. A. Guzei, R. T. Raines, *J. Am. Chem. Soc.* **2010**, *132*, 10857 – 10865.
[12] a) K. Inouye, S. Sakakibara, D. J. Prockop, *Biochim. Biophys. Acta Protein Struct.* **1976**, *420*, 133 – 141; b) K. Inouye, Y. Kobayashi, Y. Kyogoku, Y. Kishida, S. Sakakibara, D. J. Prockop, *Arch. Biochem. Biophys.* **1982**, *219*, 198 – 203.
[13] a) Y. Nishi, S. Uchiyama, M. Doi, Y. Nishiuchi, T. Nakazawa, T. Ohkubo, Y. Kobayashi, *Biochemistry* **2005**, *44*, 6034 – 6042; b) M. Doi, Y. Nishi, S. Uchiyama, Y. Nishiuchi, H. Nishio, T. Nakazawa, T. Ohkubo, Y. Kobayashi, *J. Pept. Sci.* **2005**, *11*, 609 – 616.

[14] a) K. Okuyama, *Connect. Tissue Res.* **2008**, *49*, 299 – 310; b) K. Okuyama, X. Xu, M. Iguchi, K. Noguchi, *Biopolymers* **2006**, *84*, 181 – 191.
[15] G. Porod in *Small Angle X-ray Scattering* (Eds.: O. Glatter, O. Kratky), Academic Press, New York, **1982**, pp. 17 – 51.
[16] G. Beaucage, *J. Appl. Crystallogr.* **1996**, *29*, 134 – 146.
[17] D. Motooka, K. Kawahara, S. Nakamura, M. Doi, Y. Nishi, Y. Nishiuchi, Y. K. Kang, T. Nakazawa, S. Uchiyama, T. Yoshida, T. Ohkubo, Y. Kobayashi, *Biopolymers* **2012**, *98*, 111 – 121.
[18] a) C. Hongo, V. Nagarajan, K. Noguchi, S. Kamitori, K. Okuyama, Y. Tanaka, N. Nishino, *Polym. J.* **2001**, *33*, 812 – 818; b) K. Okuyama, C. Hongo, G. Wu, K. Mizuno, K. Noguchi, S. Ebisuzaki, Y. Tanaka, N. Nishino, H. P. Bächinger, *Biopolymers* **2009**, *91*, 361 – 372; c) K. Okuyama, K. Miyama, T. Morimoto, K. Masakiyo, K. Mizuno, H. P. Bächinger, *Biopolymers* **2011**, *95*, 628 – 640.
[19] D. J. Prockop, A. Fertala, *J. Struct. Biol.* **1998**, *122*, 111 – 118.
[20] a) D. Papapostolou, A. M. Smith, E. D. Atkins, S. J. Oliver, M. G. Ryadnov, L. C. Serpell, D. N. Woolfson, *Proc. Natl. Acad. Sci. USA* **2007**, *104*, 10853 – 10858; b) T. H. Sharp, M. Bruning, J. Mantell, R. B. Sessions, A. R. Thomson, N. R. Zaccai, R. L. Brady, P. Verkade, D. N. Woolfson, *Proc. Natl. Acad. Sci. USA* **2012**, *109*, 13266 – 13271.
[21] A. Aggeli, I. A. Nyrkova, M. Bell, R. Harding, L. Carrick, T. C. McLeish, A. N. Semenov, N. Boden, *Proc. Natl. Acad. Sci. USA* **2001**, *98*, 11857 – 11862.
[22] T. Gibaud, E. Barry, M. J. Zakhary, M. Henglin, A. Ward, Y. Yang, C. Berciu, R. Oldenbourg, M. F. Hagan, D. Nicastro, R. B. Meyer, Z. Dogic, *Nature* **2012**, *481*, 348 – 351.

